

# Collision dynamics of discrete soliton pair in uniform waveguide arrays

Anuj P. Lara and Samudra Roy<sup>†</sup>

Department of Physics, Indian Institute of Technology Kharagpur, Kharagpur 721302, India

In this article we numerically study the collision dynamics of a pair of discrete solitons (DSs) in a semi-infinite nonlinear waveguide array (WA). We investigate that, a co-moving pair of identical DSs heading towards each other undergo elastic collision or a discrete *breather* formation depending on the initial amplitude ( $A_0$ ) and wavenumber ( $k_0$ ) of the two colliding DSs. Under elastic collision, the DS pair emerge unscathed and form a *cross-over* state, while under *breather* formation, two DSs are fused to form a single field. We map this phenomena by iterative simulation and present a phase plot which describes regimes of *cross-over* state or *breather* formation in  $(A_0, k_0)$  parameter space. Interaction dynamics between nonidentical DSs having same amplitudes but different wavenumbers significantly deviates from that of identical DSs. In such case, varied degree of energy exchange occurs which results three distinct output states accompanied by diffractive resonant radiation (DifRR) generation due to the interaction between soliton and WA lattice. Extending our investigation to a more generalized condition by taking different amplitudes and wavenumber of DS pair, we find that an unique secondary radiation is originated due to the collision of solitons. The wavenumber of this collision-mediated radiation depends on the wavenumbers of soliton pair. Our results shed light on the different aspects of collision dynamics of identical and non-identical DS pair in nonlinear WA and useful in understanding the complex mechanism.

## I. INTRODUCTION

Optical waveguide arrays (WAs) have garnered considerable interest over the decades as a system for exploring discrete physical phenomena which are on the atomic scale and otherwise difficult to study in a laboratory environment, and as photonic components for integrated optical devices. These arrays composed of evanescently couple waveguides have been modeled by the introduction of coupled mode theory for two adjacent waveguides[1–3] and the extension thereafter to multiple waveguide systems[4, 5]. In the continuous approximation, beam propagating in nonlinear WA obeys the nonlinear Schrödinger equation and exhibit self focusing and localization [6–9]. In balance with discrete diffraction, an analogue of diffraction in continuous media [10, 11] have established optical discrete solitons (DSs), which are observed both theoretically and experimentally[12–15]. These spatial solitons however exhibit properties that are intriguing and forbidden in the case of their continuous counterpart. The discrete nature of these WAs and the periodic potential that is formed thereby, facilitates the study of many fundamental phenomena present in discrete systems like atomic and molecular lattices on a macroscopic scale. These WAs exhibit properties and phenomena like Peierls’-Nabarro potential[16], anomalous refraction and diffraction with limitation in transverse energy transportation[10], Anderson localization[17, 18] Bloch Oscillations, localized Wannier-Stark States [19, 20], Bloch-Zener Oscillation and Zener tunneling[21, 22].

With rapid progress in fabrication techniques, WAs can be designed and constructed in specific and novel structures like sinusoidally curved WAs [23], interlaced two component super-lattice as a base for binary WAs [24], and two-dimensional WAs for continuous-discrete systems with spatiotemporal solitons (3D Light Bullets)

[25], dissipative as well Ginzburg-Landau solitons, and surface solitons[26, 27]. Binary WAs further offer an optical approach to study relativistic phenomenon such as *Zitterbewegung*[28], Klien tunneling[29], Fock states[30], neutrino oscillations[31], and Dirac solitons [32] for instance. Additionally, controlling beam and pulse propagation in light bullet routing[33], discrete soliton routing by external fields[34] have been demonstrated and studied. Further progress in the recent years have been extended to the regime of plasmonics with discrete diffraction and Bloch oscillations in plasmonic waveguide arrays[35, 36]. With such a wide range of studies, the versatility of WA systems have been proven and may provide as a base for further work in the upcoming future.

In the simplest WA structure where the separation of the adjacent waveguide channel is constant, the evolution of modes in individual waveguides that are coupled with their nearest neighbour waveguides is governed by the standard coupled mode equations. These equations also take into account both the linear and nonlinear terms of the material in the individual WAs and the set of equations combined together form what is known as the discrete nonlinear Schrödiner equation (DNLSE). In such WAs, also referred to as homogeneous WAs, DSs are formed as a result of the balance between discrete diffraction and self focusing Kerr nonlinearity. Different properties of DSs have been studied over the decades since they were first observed; however the phenomenon of emission of radiation from these solitons is a recent development in comparison to all the previously stated works. This radiation, emitted by a spatial DS propagating with a transverse velocity component in an uniform WA, is aptly named discrete diffractive resonant radiation (DifRR) [37]. The formation of DifRR under a phase matching (PM) condition is analogous to the *dispersive wave* (DW) generation in its temporal counterpart [38]. DW emerges owing to the perturbation of temporal solitons by higher-

order dispersion and nonlinearity of the optical fiber. The spectral location of DW radiation is sensitive to the zero-dispersion frequency and can be tuned to excite from deep UV to far IR regime [39]. However, in WA, due to the one-dimensional (1D) lattice formed by the periodic arrangement of the waveguides, the special DS as well as the generated DifRR exist within the resulting Brillouin boundary and their wavenumbers are limited to  $-\pi$  and  $\pi$ . This results in  $2\pi$  shift in any electric field that crosses the Brillouin boundary and recoil from the opposite side yielding *anomalous recoil* [37]. An initial phase gradient or wavevector is required to “push” the DS away from a normal incidence and interact with the waveguide with a transverse component attributing exciting phenomena like DifRR. It is only natural to be curious about how two of these special DSs with opposite wavenumbers (or *push*) will interact with each other and the lattice like structure of the WA. However, very limited background studies regarding its dynamics are presented which have been mostly limited to continuous spatial solitons[40–42], and a coupled set of NLS that form vector solitons [43–46]. Of the few mechanisms and phenomenon studied regarding DS are symmetry breaking and momentum nonconservation, velocity dependent soliton merger and breather formation[47, 48], soliton collision in optically induced photonic lattice[49] and WAs with saturable nonlinearity[50]. Studies on structures that are governed by DNLSE, for example a classic ferromagnetic spin chain with *Dzyaloshinskii-Moriya* interaction [51] has also been shown to have elastic soliton-soliton interaction akin to their continuous counterparts. Additional discrete system in which similar soliton-soliton interaction have been studied are in Bose-Einstein condensates (BECs) [45, 52].

The primary focus of this study is to investigate the collision mechanism of a pair of identical and nonidentical DSs in presence of Kerr nonlinearity, while considering the recent works on DSs, namely presence of higher order diffraction and emission of DifRR. The most basic result of collision between two solitons is their emergence without any interaction. For solitons in coupled systems, namely vector solitons, it has been observed to result in inelastic collision [53], and transfer of energy between them [44, 54]. Intuitively, similar behavior can be expected for DSs and the same has been observed in the case of Kerr [47] and saturable [50] nonlinearity, where solitons are merged to form a *breather*. It is to be expected, DSs to undergo elastic collision in the WA system with Kerr nonlinearity, with the solitons emerging without any interactions other than a phase shift similar to their continuous counterparts. Based on this knowledge we perform an initial analysis of identical DSs colliding in a homogeneous WA. Of the many parameters of DSs in WAs, we find that the soliton wavenumber ( $k_0$ ) and amplitude ( $A_0$ ) determine whether the interaction yields elastic collision or a fused state through *breather* formation. A phase plot is introduced which determines the set of values ( $k_0, A_0$ ) for which elastic collision or *breather*

formation takes place. We determine the relative phase accrue by DSs under collision during propagation in WA. It is observed that, the DS interactions are accompanied by a sudden phase shift at the point of collision. The collision dynamics of two DSs of same amplitudes and different wavenumbers differs noticeably from that of two identical DSs (having same amplitude and wavenumber). A transfer of energy between solitons occur in this case akin to that of vector solitons [54]. In addition to this, a soliton with higher amplitude and initial wavenumber radiates DifRR in Fourier-space. Due to DifRR being a relatively recent development in this field, we have limited understanding of the interaction dynamics of the two DSs in the context of emitted radiation. Taking these facts into account, we focus our investigation on the most general case where two non-identical DSs (with different wavenumbers as well as amplitudes) interacts. Interestingly, the collision of two non-identical DSs yields a secondary radiation different from usual DifRR generated by either of the DS. However, the lack of momentum conservation in this interaction [47] pose a challenge in predicting and determining the properties of this additional radiation. Despite this limitation, we perform extensive simulations to analyze the collision dynamics and some new insight is gained regarding the generation of this secondary radiation.

## II. THEORY

An infinite array of identical and lossless waveguides is considered to be an ideal WA. However for practical feasibility, we chose a semi-infinite array with a large number of waveguide channels that avoid any form of boundary interaction phenomenon. The mode evolution in the  $n^{th}$  waveguide under continuous-wave excitation along nearest-neighbor evanescent coupling is governed by the DNSLE[6, 8, 9]:

$$i \frac{dE_n}{dz} + C_{(n)}^{(n+1)} E_{n+1} + C_{(n)}^{(n-1)} E_{n-1} + \gamma_n |E_n|^2 E_n = 0, \quad (1)$$

where  $E_n$  is the electric-field amplitude of the modes in the  $n^{th}$  waveguide. The range of the index  $n$  is defined within  $-N \leq n \leq N$ , thereby defining the total number of waveguides to be  $(2N + 1)$ .  $C_{(n)}^{(n+1)}$  and  $C_{(n)}^{(n-1)}$  are the coupling coefficients of the  $(n + 1)^{th}$  and  $(n - 1)^{th}$  waveguide to the  $n^{th}$  waveguide respectively with units in  $\text{m}^{-1}$ .  $\gamma_n = \omega_0 n_2 / (c A_{eff})$  is the nonlinear coefficient of an individual waveguide in units of  $\text{W}^{-1} \text{m}^{-1}$  where  $n_2$  is the Kerr coefficient and  $A_{eff}$  is the effective mode area. For a uniform WA the coupling coefficients are considered to be identical ( $C_{(n)}^{(n+1)} = C_{(n)}^{(n-1)} = C$ ). Additionally, the nonlinear coefficient ( $\gamma_n$ ) is equal for every waveguide and written as  $\gamma_n = \gamma \forall n$ , as each of the constituent waveguides are considered to be composed of the same material and have the same dimensions.

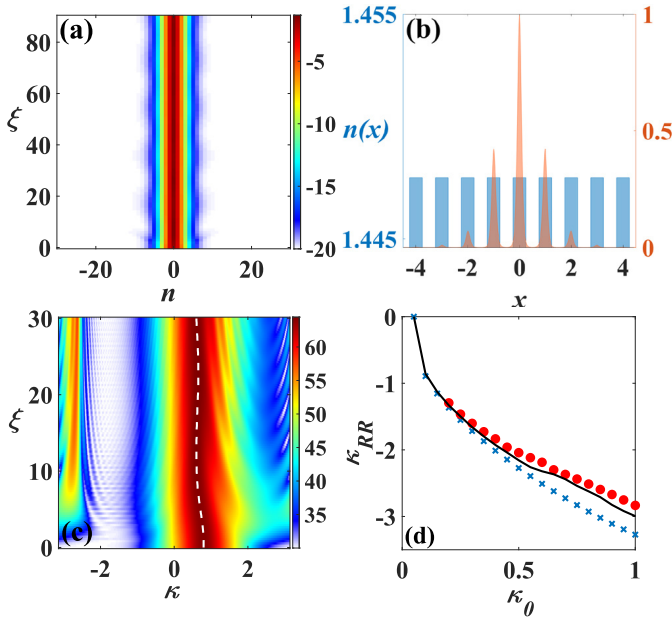


FIG. 1. (a) Formation of DS in  $n$  space propagating in a uniform WA. (b) Spatial distribution of DS at output in the background of periodic refractive index profile  $n(x)$  offered by the uniform WA. (c) Evolution dynamics of a DS in the  $\kappa$  space for an incident wavenumber of  $\kappa_0 = 0.8$  emitting a strong difRR with wavenumber  $\kappa_{RR} \approx -2.8$ . The variation of the soliton wavenumber (soliton peak) is tracked by a white dotted line. (d) Comparison between the location of generated difRR as a function of incident angle  $\kappa_0$  obtained numerically (red circles), from the PMC (crosses) and modified input for PMC (solid black line) using the average wavenumber.

For low power condition the nonlinear term can be neglected ( $\gamma = 0$ ) and Eq.(1) thereby reduces to an analytically integrable equation. The solution of single waveguide excitation in such a case leads to mode evolution that exhibit discrete diffraction with the solution in the form of  $E_n(z) = E_n(0)i^n J_n(2Cz)$ , where  $J_n$  is the Bessel function of order  $n$ [11]. Physically, the varying  $z$  dependent phase shift is the underlying reason for discrete diffraction. Intuitively, one can understand the formation of solitons by counteracting this discrete diffraction by a balancing Kerr induced self focusing[6]. Fig.1(a) describes such a soliton forming and propagating in nonlinear uniform WA. In Fig.1(b) the spatial distribution of the DS is illustrated in the background of periodic refractive index grid offered by the typical WA. The DNLSE can be converted to an useful normalized form through the following transformations  $E_n \rightarrow \sqrt{P_0}\psi_n$ ,  $\gamma P_0 z \rightarrow \xi$ , and  $C/(\gamma P_0) \rightarrow c$ :

$$i \frac{d\psi_n}{d\xi} + c [\psi_{n+1} + \psi_{n-1}] + |\psi_n|^2 \psi_n = 0, \quad (2)$$

where  $P_0$  is the associated peak beam power in units of Watt. It is to be noted that the total power flowing through the array,  $P = \sum_n |\psi_n|$  and Hamiltonian,

$H = \sum_n [c|\psi_n - \psi_{n-1}|^2 - \gamma|\psi_n|^2/2]$  remain conserved during the propagation[16] under idealized scenario (no losses and continuous wave excitation). In the linear case, exploiting the discrete plane-wave solution  $\psi_n(\xi) = \psi_0 [i(nk_x d + \beta\xi)]$  of Eq.2, one can obtain the dispersion relation between  $\beta$  and  $k_x$  as

$$\beta(\kappa) = 2c \cos(\kappa) + |\psi_0|^2, \quad (3)$$

where  $d$  is the separation between two adjacent waveguides,  $k_x$  is the transverse wave vector and  $\kappa \equiv k_x d$  is the phase difference between two adjacent waveguides[6]. The transverse component ( $\kappa$ ) undergoes a phase gain  $\phi_t = \beta(\kappa)\xi$  during it's propagation which leads to the transverse shift of the propagating beam  $\Delta n = \partial\phi_t/\partial\kappa$ [55]. Hence, the beam propagates at an angle  $\theta = \tan^{-1} [\partial\beta(\kappa)/\partial\kappa] = \tan^{-1} [-2c \sin(\kappa)]$ [56]. The Taylor expansion of  $\beta(\kappa)$  about the incident wavenumber ( $\kappa_0$ ) results in the diffraction relation:

$$\beta(\kappa) = \beta(\kappa_0) + \sum_{m \geq 1} \frac{D_m}{m!} \Delta\kappa^m \quad (4)$$

where  $D_m \equiv (d^m \beta/d\kappa^m)|_{\kappa_0}$  and  $\Delta\kappa = \kappa - \kappa_0$ . Performing a Fourier transformation to change the domain as  $\kappa \rightarrow n$  by replacing  $\Delta\kappa \equiv -i\partial_n$ , where  $n$  is defined as a continuous variable of an amplitude function  $\Psi(n, \xi) = \psi_{n,\xi} \exp(-i\kappa_0 n)$ , we have an approximate standard nonlinear Schrödinger equation(NLSE)[37]

$$\left[ i\partial_\xi - \frac{D_2}{2} \partial_n^2 + \sum_{m \geq 3} \frac{D_m}{m!} (-i\partial_n)^m + |\psi(n, \xi)|^2 \right] \psi(n, \xi) = 0 \quad (5)$$

Defining  $n$  as a continuous variable can be justified by the fact that the involved solitons encompass several waveguides. By using the concept of co-moving frame  $n \rightarrow n + D_1 \xi$  and introducing a phase evolution substitution  $\psi(n, \xi) = \psi(n, \xi) \exp [i\beta(\kappa_0)n]$  we can eliminate the first and second term of the Taylor expansion. A soliton solution

$$\psi_{sol} = \psi_0 \operatorname{sech} \left( \frac{n\psi_0}{\sqrt{|D_2|}} \right) \exp (ik_{sol}\xi) \quad (6)$$

can be obtained for Eq.5 for  $D_{m \geq 3} = 0$ , with  $k_{sol} \equiv \psi_0^2/2$  being the longitudinal wavenumber of the soliton. Note that a bright soliton exists only when condition  $|\kappa_0| < \pi/2$  or  $2c \cos(\kappa_0) > 0$  is satisfied. Inserting the plane-wave solution  $\exp [i(k_{lin}\xi + \Delta\kappa n)]$  in a linearized Eq.5 we obtain the dispersion relation

$$k_{lin}(\Delta\kappa) = \beta(\kappa) - \beta(\kappa_0) - D_1 \Delta\kappa. \quad (7)$$

A soliton of the form in Eq.(6) emits a radiation in  $\kappa$ -space by transferring energy to the linear wave when the condition  $k_{sol} = k_{lin}(\Delta\kappa)$  is satisfied. This is the PM

condition required for generating DifRR [37], which can be further expressed as,

$$[\cos(\kappa) - \cos(\kappa_0) + \sin(\kappa_0)\Delta\kappa] = \tilde{\psi}_0^2 \quad (8)$$

where  $\tilde{\psi}_0 = \psi_0/2\sqrt{c}$ . The solution to this relation gives the wavenumber of the generated DifRR ( $\kappa_{RR} = \kappa_0 + \Delta\kappa$ ) as a function of the soliton wavenumber  $\kappa_0$ . In Fig. 1(c), the formation of the DifRR in  $\kappa$ -space is illustrated for initial wavenumber  $\kappa_0 = 0.8$ . It is to be noted that the generated DifRR is also subjected to same limits ( $\kappa < |\pi|$ ) within the first Brillouin zone and undergo a shift in its wavenumber by  $\pm 2\pi$ . In Fig. 1(d) we plot the wavenumber ( $\kappa_{RR}$ ) of DifRR as a function of initial soliton wavenumber  $\kappa_0$ . However, it is observed that  $k_{RR}$  obtained from numerical simulation deviate from the result predicted by the PM condition when  $k_0$  is relatively large. It can be noted that, the recoil of the soliton after emitting the radiation is significant for higher values of  $k_0$  resulting a change in its wavenumber. We track this change of soliton wavenumber as marked by the white dotted line in Fig. 1 (c). Under the assumption that soliton wavenumber undergoes a change from  $\kappa_0$  to  $\kappa'_0$ , we replace the average wavenumber  $\kappa_0 \rightarrow (\kappa'_0 + \kappa_0)/2$  in the PM condition Eq. 8 and find a better agreement with numerical results as shown by the solid black line in Fig. 1 (d).

### A. Soliton Collision in DNLS Systems

Solitons by nature maintain their shape and location during propagation. This property is also known to extend to collisions between two solitons in continuous domain where they interact on collision and appear to pass through each other. After such a collision the solitons undergo an instant translation in space and/or time and defined as a phase shift. This property was originally observed in a study of Korteweg-de-Vries (KdV) equation and later in systems governed by NLSE[41]. As established, two solitons simultaneously launched with their peaks at two different locations will maintain their position while propagating. A transverse motion in the solitons is initiated by a “push” in the form of a phase gradient  $k$  across the solitons at their inputs[47]. Two solitons with appropriate opposite signs of phase gradient  $k$  can be made to collide with their transverse velocities proportional to  $k$ . Such a pair of DSs at the input is given by,

$$\begin{aligned} \psi(n, 0) = & A_1 \operatorname{sech} \left[ \frac{A_1(n - n_1)}{\sqrt{2c \cos k_1}} \right] \exp [ik_1(n - n_1)] \\ & + A_2 \operatorname{sech} \left[ \frac{A_2(n - n_2)}{\sqrt{2c \cos k_2}} \right] \exp [ik_2(n - n_2)], \end{aligned} \quad (9)$$

where  $n_{j=1,2}$  are the location of the DS peaks,  $A_{j=1,2}$  are the amplitudes and  $k_{j=1,2}$  are the respective wavenumbers. These four parameters are real and their signs

determines whether the solitons will travel in opposite directions or towards each other while they propagate. One valid combination is negative signs of  $k_1$  and  $n_2$ , and positive  $k_2$  and  $n_1$ . It is to be noted that the reversal of their signs is also a valid combination, however the results obtained merely mirror the phenomenon observed in the initial case. The DSs after a collision either emerge with their properties intact or fuse together to form a *breather* [[41, 57]]. The results of the collision are determined and controlled by the soliton amplitude  $A_j$  and wavevector  $k_j$ , where  $j = 1, 2$ . In subsequent sections we will analyse the deeper aspects of the collision dynamics and other related phenomena along with the results of numerical analysis.

### B. Waveguide Array Design

Before we proceed to a detailed analysis of collision dynamics, we define a physically realizable waveguide structure by utilizing the facility of fs laser based writing in transparent bulk media[58, 59]. This enables us to prepare a WA composed of  $\text{GeO}_2$  doped silica cores suspended in a silica cladding as illustrated in Fig.2 (a). The refractive indices of the core and cladding are  $n_1 \approx 1.4477$  and  $n_2 \approx 1.4446$ , respectively, at the operating wavelength  $\lambda_0 = 1.55 \mu\text{m}$ . We consider cylindrical cores with radius  $r = 5 \mu\text{m}$ , separated by a distance  $d = 20 \mu\text{m}$  with a calculated nonlinear coefficient of  $\gamma = 0.79 \text{ W}^{-1}\text{km}^{-1}$  for the given geometry. For such a WA arrangement, the

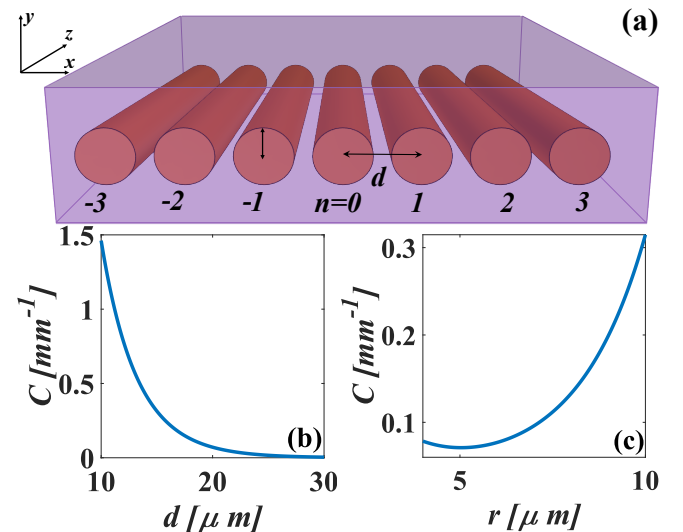


FIG. 2. (a) Schematic representation of the proposed WA with cylindrical cores of radius  $r$ , where adjacent waveguides are uniformly separated by  $d$ . (b) Variation of coupling coefficient as a function of separation between adjacent waveguides for  $r = 5 \mu\text{m}$ . (c) Variation of coupling coefficient as a function of core radius for a fixed separation  $d = 20 \mu\text{m}$ .

coupling coefficient between adjacent waveguides is given

by[60]

$$C(d, r) = \frac{\lambda_0}{2\pi n_1} \frac{U^2}{r^2 V^2} \frac{K_0(Wd/r)}{K_1^2(W)}, \quad (10)$$

where  $\lambda$  is the free space wavelength, and  $K_\nu$  are the modified Bessel functions of the second kind of order  $\nu$ .  $U$  and  $V$  are the mode parameters that satisfy  $U^2 + W^2 = V^2$ , where the  $V$  parameter is defined as  $V = k_0 r \sqrt{n_1^2 - n_2^2}$ , and  $U$  is approximated as  $U \approx 2.405 e^{-(1-\Delta/2)/V}$ , with  $\Delta = 1 - (n_2/n_1)^2$ [61]. Here,  $r$  is the core radius,  $k_0 (= 2\pi/\lambda_0)$  is the free space wavevector and  $d$  represents the separation between two adjacent waveguides. The variation of the coupling coefficient as a function of separation  $d$  for a fixed radius  $r$  and vice versa is plotted in Fig.2(b)(c). In our numerical analysis we consider a homogeneous WA composed of waveguides with radius  $r = 5 \mu\text{m}$  and separation  $d = 20 \mu\text{m}$ . For these parameters we obtain the value of the coupling coefficient to be  $\approx 0.07 \text{ mm}^{-1}$ .

### III. NUMERICAL ANALYSIS

In this section we numerically investigate the results of interaction between two DSs defined by Eq.9 in a uniform homogeneous WA described in Fig.2 (a). We consider a WA with the range of its  $n$  index as  $-350 \leq n \leq 350$  which defines  $N = 350$  and a total of  $2N + 1 = 701$  waveguides in the array.

#### A. Collision of two identical DSs

A pair of identical DSs are defined by taking  $k_0 = k_2 = -k_1$  and  $A_{j=1,2} = A_0$ , reducing Eq.9 to,

$$\begin{aligned} \psi(n, 0) = & A_0 \operatorname{sech} \left[ \frac{A_0(n + n_0)}{\sqrt{2c \cos k_0}} \right] \exp[-ik_0(n - n_0)] \\ & + A_0 \operatorname{sech} \left[ \frac{A_0(n - n_0)}{\sqrt{2c \cos k_0}} \right] \exp[ik_0(n - n_0)]. \end{aligned} \quad (11)$$

In addition, the location of soliton peaks are  $n_0 = n_1 = -n_2$  in accordance to the collision condition stated earlier and to place them equidistant from the central waveguide ( $n = 0$ ) in the array. In continuous limit the total energy of soliton pair is  $E = 4A_0\sqrt{2c \cos(k_0)}$ . The evolution and collision dynamics of such a pair for DSs with initial wavenumber  $k_0 = 0.3$ , starting at  $n_0 = 20$  for two different amplitudes  $A_0 = 0.8$  and  $0.5$ , are illustrated in Fig.3. In Fig.3(a),(b) we observed the evolution of the soliton pair in the  $n$  and  $\kappa$  domain, respectively for  $A_0 = 0.5$ , where they interact and emerge while maintaining their shape and properties under an elastic like collision. Numerically, we find the energy carried by each DS,  $E = 2A_0\sqrt{2c \cos(k_0)} = 1.514$  remains conserved throughout the propagation. The spectrogram plot in

Fig.3 (c) at output reflects how two DS remain intact followed by an elastic like collision. To visualize the complete picture see Supplemental Material [62]. However, the DS pair are fused together to form a discrete *breather* when we increase the amplitude to  $A_0 = 0.8$  (keeping  $k_0 = 0.3$ , same as before). The formation of this fused state is shown in Fig.3 (d) and (e). The spectrogram in  $(n-k)$  space, as shown in Fig.3 (f), depicts the formation of the single state where we also observe side-lobes exhibiting multiple weak radiations. To visualize the complete picture see Supplemental Material [63].

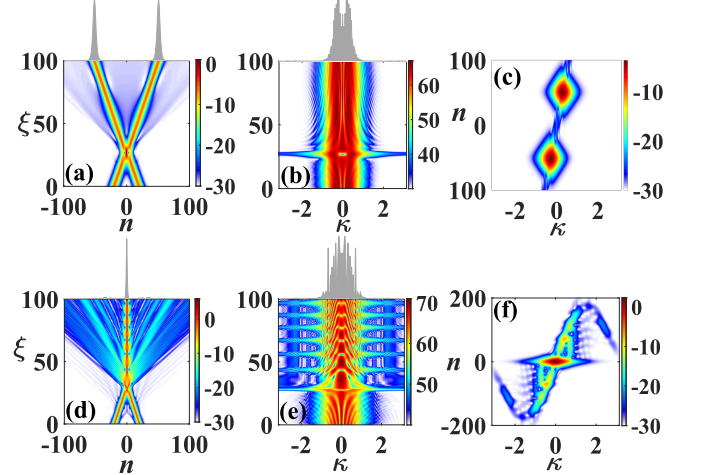


FIG. 3. Evolution of two identical DS pair launched in a WA obliquely with  $k_0 = 0.3$  towards each other. Evolution in (a)  $n$  and (b)  $\kappa$  domains (b) for amplitude  $A_0 = 0.5$  result in a crossover state followed by an elastic like collision. (c) Spectrogram at output ( $\xi = 100$ ) showing two distinct DSs in  $(n-k)$  space. (d) Two DS of amplitude  $A_0 = 0.8$  launched with the same value of  $k_0$  merge together to form a *breather* with small side-lobes. (e) Evolution of the breather in  $\kappa$ -space. (f) Spectrogram at output showing the single merge state where the side-lobes are distributed in  $n$  and  $\kappa$  domain in the form of multiple weak radiation.

In a detailed analysis it is found that the result of the interaction between the soliton pair (elastic collision or *breather* formation) is dependent on the relative values of soliton amplitude  $A_0$  and initial wavenumber  $k_0$  only. By compiling the results for over a range of  $A_0$  and  $k_0$  we map the values for which *breather* formation does and doesn't take place and represent it in the form of a phase map in Fig.4. A band formed on this parameter space corresponds to the values of  $A_0$  and  $k_0$  for which DSs merger or *breather* formation takes place. In addition, to shed more light on the collision dynamics, we further study the evolution of relative phase and peak power of the DSs (and *breather*) for the both cases. In time domain, the average soliton phase at a point in the propagation axis ( $\xi$ ) is defined as [64],

$$\phi(\xi) = \tan^{-1} \left( \frac{\int |\psi(t, \xi)|^2 \operatorname{Im}[\psi(t, \xi)] dt}{\int |\psi(t, \xi)|^2 \operatorname{Re}[\psi(t, \xi)] dt} \right), \quad (12)$$

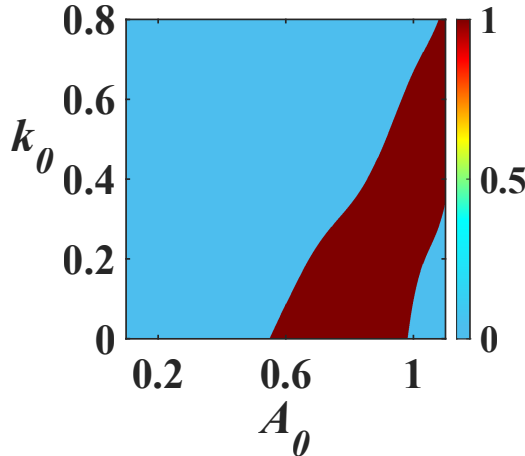


FIG. 4. A phase map for *breather* formation as function of  $A_0$  and  $k_0$  with the values of *breather* formation denoted by the region marked in red. For other set of values  $(A_0, k_0)$  on this phase map, soliton interaction result in elastic collision.

with the contribution to the average phase being limited to near pulse electric field by a pulse intensity weight  $|\psi(\xi, t)|^2$ [64]. We consider the fact that the NLSE in spatial domain is analogous to its temporal counterpart and rewrite this equation in terms of  $n$  ( $t \rightarrow n$ ). Discretizing the Eq. (12) by the approximation  $dn \rightarrow 1$ , we obtain.

$$\phi(\xi) = \tan^{-1} \left( \frac{\sum |\psi_n(\xi)|^2 \text{Im}(\psi_n(\xi))}{\sum |\psi_n(\xi)|^2 \text{Re}(\psi_n(\xi))} \right). \quad (13)$$

Note, the average “lattice” phase for a pure DS (with  $k_0 = 0$ ) oscillates between  $\pi/2$  to  $-\pi/2$  as it progresses along  $\xi$ . This is attributed to the range  $(-\pi/2, \pi/2)$  of the  $\tan^{-1}$  function. This repetition is periodic in a case of a standard DS, and on unwrapping the value of  $\phi(\xi)$  i.e adding  $\pi$  to the value of  $\phi(\xi)$  whenever it emerges from the other side of the domain, we obtain  $\phi(\xi)$  as a linear function of  $\xi$ [64]. We similarly calculate the average phase of the system for both the cases of elastic collision and *breather* formation ( $\phi_k(\xi)$ ), then take the difference between it and that of the pure DS ( $\phi_0(\xi)$ ) which is considered to be a reference phase. The evolution of the relative phase  $\phi_k(\xi) - \phi_0(\xi) = \Delta\phi(\xi)$  helps us to achieve a better resolution if any phase change occurs during the interaction between the DS pair. We simultaneously calculate the evolution of the peak power in the system which is defined as  $P_0 (= |\psi_{\max}|^2)$ , where  $\psi_{\max}$  is the maximum of the total field in the WA. The evolution of average phase and peak power for both types of interaction are illustrated in Fig.5. Fig.5(a) and (c) show the variation of  $\Delta\phi$  and  $P_0$  (in same frame) for elastic collision of the DS pair. It is evident that the relative average phase which changes uniformly experiences an abrupt shift at collision point. This location is further corroborated by a change in the peak power of the system as observed in Fig.5(c). No such abrupt change in the

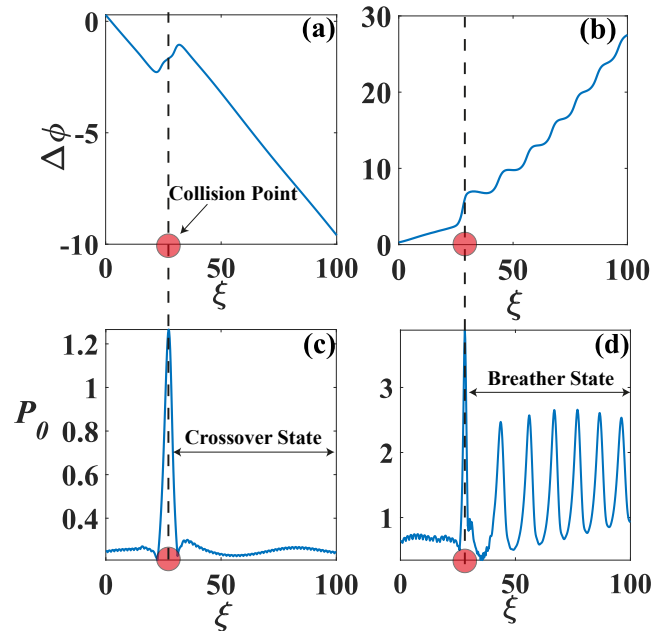


FIG. 5. Evolution of (a),(b) relative phase and (c),(d) peak power for elastic collision [(a) and (c)] and breather formation [(b) and (d)]. Point of collision is accompanied by a spike in (c) peak power and (a) abrupt change in phase evolution. For a *breather* formation, peak power oscillates periodically (d) reciprocating (b) the step-wise increase in phase. Point of collision at  $\xi$  is represented by a dotted line and red circle in each case.

peak power and phase are observed after collision, ensuring a crossover state where two DS emerges with out any change in its shape. A similar comparison of the relative phase and peak power, in the case of *breather* formation are illustrated in Fig.5 (b) and (d). For fused state, we observe the formation of periodic “lumps” in the relative phase evolution and successive spikes in peak power. These periodic lumps (in  $\Delta\phi$ ) and successive spikes (in  $P_0$ ) ensure the *breather* formation and indicate the locations where the *breather* resulting from the collision emits a pair of radiation (in  $k$ -space) that spread in opposite directions (in  $n$ -space) as side-lobes. The first lump and peak are generated at the point of collision between two DSs heading towards each other.

## B. Collision of two non-identical DS

Collision of identical DS is a special case, where the solitons are exactly identical and have the same and opposite transverse velocities. The natural extension to this case is a generalized study of two DSs having unequal amplitudes and different initial wavenumbers as described in Eq.9. We split this study into two parts, namely (a) solitons with equal amplitudes ( $A_1 = A_2$ ) and nonidentical wavenumbers ( $|k_1| \neq |k_2|$ ), and (b) both parameters of the solitons are unequal ( $A_1 \neq A_2 \& |k_1| \neq |k_2|$ ). At a

glance, it is evident from the soliton solution that solitons with non-identical wavenumbers and equal amplitudes will have different width proportional to  $\sqrt{\cos(k_{j=1,2})}$ . This results in the solitons being nonidentical with dif-

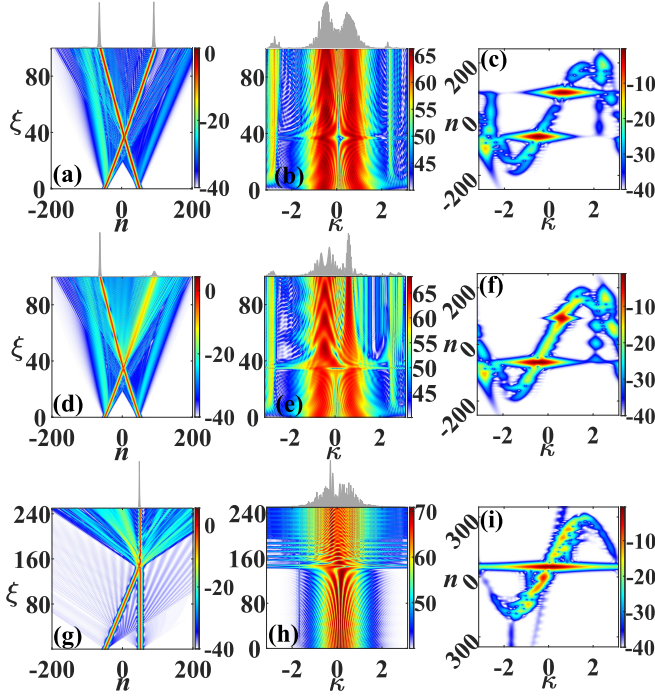


FIG. 6. Collision of two DSs with non-identical wavenumbers ( $|k_1| \neq |k_2|$ ) and equal amplitudes. Collision dynamics of DS pair in (a)  $n$ - space (b)  $\kappa$ - space and (c) corresponding output spectrogram for the set of parameter  $k_1 = 0.9$  and  $k_2 = -0.7$ . Collision dynamics of DS pair in (d)  $n$ - space (e)  $\kappa$ - space and (f) corresponding output spectrogram for the set of parameter  $k_1 = 0.9$  and  $k_2 = -0.6$ . Formation of the *fused state* in (g)  $n$ - space (h)  $\kappa$ - space and (i) corresponding output spectrogram for the set of parameter  $k_1 = 0.3$  and  $k_2 = 0$ . In all the ceases  $n_0 = 50$ .

ferent widths while having the same amplitudes. We observe three distinct collision dynamics when DS pair with different  $k$  values are allowed to interact. Depending on the relative value of initial wavenumber  $k$ , either we have a cross-over state resulting two almost identical DS or two distinctly different DSs at the output. With suitable  $k$  values it is even possible to excite a fused state showing a single soliton at output. To excite crossover states, we consider the wavenumber of one DS to be  $k_1 = 0.9$ , while taking  $k_2 = -0.6$  and  $-0.7$ , and allow these DS to collide. The entire collision dynamics is illustrated in Fig.6 (a)-(f). For the set ( $k_1 = 0.9$  &  $k_2 = -0.7$ ), we observe a negligible exchange of energy between the DS pair. Nothing of interest occurs in the corresponding wavenumber domain ( $\kappa$ -space) except the generation of DifRR exhibiting two strong side-bands (see Fig. 6 (b)). The spectrogram in Fig. 6 (c) indicates the preservation of the DS pair and corresponding DifRR recoiled by the Brillouin boundary. However strikingly different

dynamics is observed for the other set of parameters i.e ( $k_1 = 0.9$  &  $k_2 = -0.6$ ), where a significant amount of energy is taken away by one DS and the other emerges with a lower amplitude and is broadened in space (see Fig. 6 (c)-(f)). Simultaneously, the soliton that lost its energy undergoes a narrowing in width in the wavenumber domain ( $\kappa$ -space) as observed in Fig.6(e). Additionally, relatively strong radiations appear over a broad region in wavenumber domain and are located at different positions in the spatial domain, with some overlapping. We follow this up with a detailed numerical analysis considering a finer variation in the wavenumbers. However we observe that, the amount of energy transfer between the solitons is highly sensitive to the relative values of  $k_1$  and  $k_2$  does not follow a pattern in the terms of  $k_1$  and  $k_2$ . Furthermore, the behavior of energy transfer is also dependent upon the launching location  $n_0$  of the soliton. Non-identical soliton pair also forms a fused-state exhibiting a single soliton at output. In Fig.6(g)-(i) we illustrate the formation of the fused-state while taking  $k_1 = 0.3$  and  $k_2 = 0$ . The spectrogram in Fig.6(i) exhibits the formation of the fused state with side-lobes at output.

Next we consider the most general case where the DSs have unequal amplitudes ( $A_1 \neq A_2$ ) and initial wavenumbers ( $|k_1| \neq |k_2|$ ). We introduce a scaling parameter  $H$  to define one of the DS amplitudes ( $A_2 = HA_1$ ) as function of the other ( $A_1$ ). With this substitution we rewrite Eq.11 as,

$$\begin{aligned} \psi(n, 0) = & A_1 \operatorname{sech} \left[ \frac{A_1(n - n_1)}{\sqrt{2c \cos(k_1)}} \right] \exp [ik_1(n - n_1)] \\ & + HA_1 \operatorname{sech} \left[ \frac{HA_1(n - n_2)}{\sqrt{2c \cos(k_2)}} \right] \exp [ik_2(n - n_2)], \end{aligned} \quad (14)$$

while maintaining the combination of  $n_{j=1,2}$  and  $k_{j=1,2}$  required for the DSs to collide. As an initial study, we analytically determine the total energy flowing through the array with a continuous assumption as  $E = \int_{-\infty}^{\infty} |\psi(n)|dn$  and obtain the total energy in the system at input as

$$E = 2A_1\sqrt{2c \cos(k_1)} + 2HA_1\sqrt{2c \cos(k_2)}. \quad (15)$$

We numerically determine the output energy by exploiting the expression  $E = \sum_n |\psi_n|^2$ . For the set of parameters  $c = 1.2$ ,  $A_1 = 0.8$ ,  $H = 0.3$ ,  $k_1 = 0.7$ , and  $k_2 = -0.8$ , we numerically calculate the total energy at output as  $E = 2.7885$  which is consistent with Eq.15 ensuring the conservation of energy. Proceeding ahead, we launch a pair of non-identical DS defined by Eq.14 in the proposed WA structure as shown in Fig.2(a). In Fig.7 (a),(b) we present the mesh plot showing the collision dynamics in  $n$  and  $\kappa$ -space, respectively. It can be seen in Fig.7(a) and (b) that the DS with the larger amplitude  $A_1$  almost immediately starts emitting a strong DifRR (labeled as 1) whose location in the  $\kappa$ -domain can be predicted by Eq.8. The other DS of the pair doesn't radiate any DifRR,

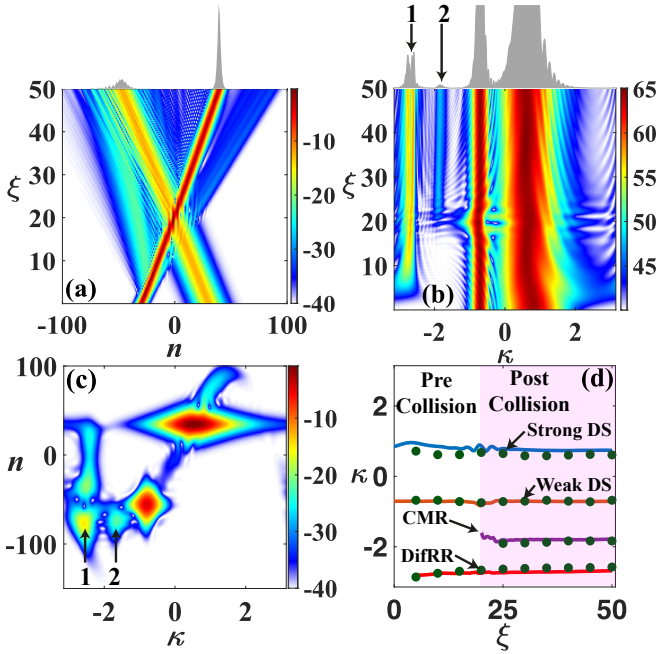


FIG. 7. Collision dynamics of two non-identical DSs illustrated in (a)  $n$ -space and (b)  $\kappa$ -space. (c) Spectrogram at output. The the locations of DifRR (1) and secondary radiation (2) are indicated by arrows. The wave vectors of the two DSs are  $k_1 = 0.8$  and  $k_2 = -0.7$  respectively, with  $H = 0.3$ . Plot (d) describes the evolution of wavenaumbers for four fields, DS pair, DifRR and collision mediated radiation (CMR). The solid lines describe the wavenumbers ( $\bar{\kappa}_j$ ) derived by the *center of mass* technique. The corresponding numerical results are depicted by solid dots.

however an additional component is observed in the  $\kappa$ -domain with a relatively small amplitude (labeled as 2 Fig.7(b)). This secondary radiation is originated as a result of the collision between the DS pair having different initial wavenumber. It is observed that, the origin of this weak radiation can be traced with better resolution when we allow two non-identical (having different strength and wavenumber) DS to collide. The XFR OG diagram shown in Fig.7(c) captures this collision mediated weak radiation. We can discern that this radiation is in fact *sandwiched* by overlapping with the primary radiation (DifRR) and the weak DS in the  $n$ -space. To visualize the complete picture see Supplemental Material [65]. It is to note that, the emission of radiations results in minor variation in wavenumbers of the propagating waves. Numerically one can calculate the variation of the wavenumber by simply track the peak value of  $\tilde{\psi}_j(\kappa, \xi)$  which is the Fourier transform of the original field,  $\psi_j(n, \xi) \rightarrow \tilde{\psi}_j(\kappa, \xi)$ . However the problem can be addressed semi-analytically by exploiting the standard technique of calculating center of mass. Thus the resulting wavenumber of the  $j^{th}$  wave  $\bar{\kappa}_j(\xi)$  can simply be expressed as [66],  $\bar{\kappa}_j(\xi) = \int_{\kappa_i}^{\kappa_f} \kappa |\tilde{\psi}_j(\kappa, \xi)|^2 d\kappa / \int_{\kappa_i}^{\kappa_f} |\tilde{\psi}_j(\kappa, \xi)|^2 d\kappa$ , where  $\kappa_i$  and  $\kappa_f$  determines the range of the distribution of  $\tilde{\psi}_j(\kappa)$

in  $\kappa$ -space. In Fig.7(d) we depict the variation of  $\bar{\kappa}_j(\xi)$  of four different waves (strong DS, weak DS, DifRR and weak secondary radiation) before and after collision. The solid dots represent the corresponding values obtained numerically.

This collision mediated secondary radiation is found to be tailored by the initial wavenumbers of the DS pair. To study the dependence, we fix the initial wavenumber of the strong DS ( $k_1$ ) and vary the input wavenumber ( $k_2$ ) of the weak DS (having lower amplitude). To illustrate the variation of weak radiation we define the wavenumber difference  $\delta k = k_1 - k_2$ , and vary  $k_2$  over a range within the DS formation condition ( $k_2 < |\pi/2|$ ). The locations of both the primary and secondary radiations in the wavenumber domain for two different values of  $k_1 = 0.9, 0.7$  are plotted as a function  $\delta k$  in Fig.8(a). As expected, the location of the primary radiation (generated by the strong DS) for both the values of  $k_1$  doesn't change with  $\delta k$  and it's location can be estimated exploiting Eq.8 as represented by the dotted lines in Fig.8(a).

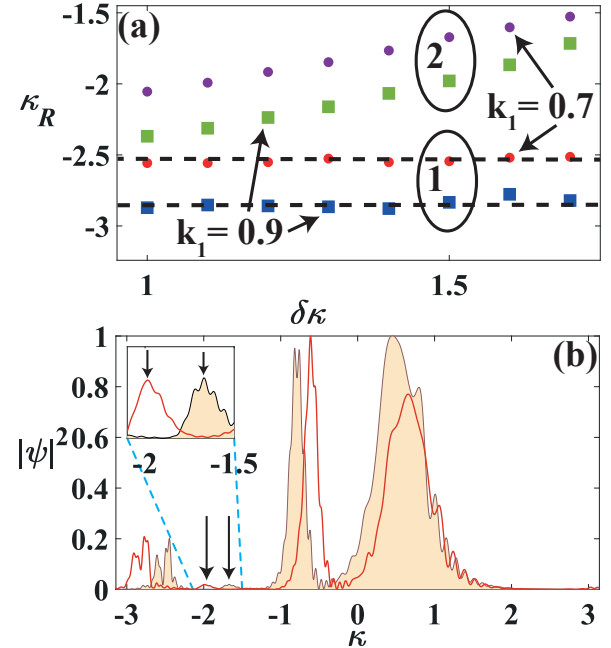


FIG. 8. (a) The locations of DifRR (1) and secondary radiation (2) as a function of  $\delta k$ . The wavenumber of the secondary radiation varies with  $\delta k$  but also depends on  $k_1$ . (b) Distribution of the DS pair at output in  $\kappa$ -space for two set of  $k$  (keeping  $\delta k$  same). For shaded curve ( $k_1 = 0.6, k_2 = -0.9$ ) and for unshaded curve ( $k_1 = 0.8, k_2 = -0.7$ ). Strong DifRR and weak CMRs (marked by arrows) are evident. The separation of the weak radiation is highlighted in the inset.

The collision mediated secondary radiation, however, exhibits almost a linear relationship with  $\delta k$ . The formation of the weak radiation in  $\kappa$ -space is characteristically different from that of the usual difRR [37] and indeed difficult to frame analytically as it depends on various parameters like  $k_1$  and  $k_2$ . From Fig.8(a) it is evident that the location of weak radiations ( $\kappa_R$ ) is

not same for the same value of  $\delta k$ , when  $k_1$  differs. To grasp this phenomenon, in Fig.8(b) we plot the output of the DS collision (in  $\kappa$ - space) exhibiting strong (pure DifRR) and weak (collision mediated) radiations (highlighted in the inset). Keeping  $\delta k$  fixed two set of DS pairs, ( $k_1 = 0.8, k_2 = -0.7$ ) and ( $k_1 = 0.6, k_2 = -0.9$ ) are launched and we capture the output in the same frame for comparison. It is evident from Fig. 8 (b) that, even for the same value of  $\delta k (= 1.5)$  the wavenumber of the collision mediated weak radiations (indicated by arrows) differ significantly for two set of DS pair. Hence the wavenumber of the CMR not only depend on the  $\delta k$ , but the relative values of DS wavenumbers.

#### IV. CONCLUSION

A spatial discrete soliton emits diffractive resonance radiation when launched with an initial wavenumber in a semi-infinite uniform waveguide array. The situation becomes even interesting when two such solitons are allowed to collide with each other by inserting a *push* through initial wavenumber resulting an oblique incidence. We numerically investigate the complex collision dynamics of varied types of spatial DS pairs, staring from the simplest case of identical DS pair, to a more generalized combination of soliton pairs. The collision of the identical DS pair, either forms (*i*) a fused *breather* state or (*ii*) a cross-over state (followed by an elastic like collision) depending on the relative values of initial amplitudes ( $A_0$ ) and wave

number ( $k_0$ ) of the solitons. Performing extensive iterative simulation we map this entire process by depicting a phase plot in parameter  $(k_0, A_0)$  space where the region of *breather* formation is indicated by a band. The relative phase difference measurement also results in very different observations for *breather* formation and cross-over state. When for a crossover state, the relative phase changes monotonically with negative value, the *breather* formation attributes a positive increment in phase. Also it is noticed that the phase changes abruptly at collision points. The interaction for two non-identical soliton with different wavenumber is found to be interesting as three distinct states are formed. In an addition to the usual *breather* state, two different cross-over states are formed where degree of energy exchange between solitons differs significantly. By extending this study to a more generalized condition of both DSs having different amplitudes and wavenumbers, we observe the formation of a collision mediated secondary radiation along with usual DifRR from one of the solitons. The wavenumber of the secondary radiation depends on the relative wavenumber of DS pair. In conclusion we can say, collision of spatial DSs in discrete media yields a very diverse range of interesting phenomena and in our study we try to shed light on few of them.

#### ACKNOWLEDGMENT

A.P.L. acknowledges University Grants Commission, India for support through Junior Research Fellowship in Sciences, Humanities and Social Sciences (ID 515364)

---

[1] S. E. Miller, Bell System Technical Journal **33**, 661 (1954).

[2] A. Yariv, IEEE Journal of Quantum Electronics **9**, 919 (1973).

[3] U. Das, Y. Chen, and P. Bhattacharya, Applied Physics Letters **51**, 1679 (1987).

[4] H. Haus and L. Molter-Orr, IEEE Journal of Quantum Electronics **19**, 840 (1983).

[5] N. Finlayson and G. I. Stegeman, Applied Physics Letters **56**, 2276 (1990).

[6] D. N. Christodoulides and R. I. Joseph, Optics Letters **13**, 794 (1988).

[7] J. E. Sipe and H. G. Winful, Optics Letters **13**, 132 (1988).

[8] Y. S. Kivshar and D. K. Campbell, Physical Review E **48**, 3077 (1993).

[9] Y. S. Kivshar, Optics Letters **18**, 1147 (1993).

[10] T. Pertsch, T. Zentgraf, U. Peschel, A. Bräuer, and F. Lederer, Physical Review Letters **88**, 093901 (2002).

[11] H. S. Eisenberg, Y. Silberberg, R. Morandotti, A. R. Boyd, and J. S. Aitchison, Physical Review Letters **81**, 3383 (1998).

[12] H. S. Eisenberg, R. Morandotti, Y. Silberberg, J. M. Arnold, G. Pennelli, and J. S. Aitchison, Journal of the Optical Society of America B **19**, 2938 (2002).

[13] U. Peschel, R. Morandotti, J. M. Arnold, J. S. Aitchison, H. S. Eisenberg, Y. Silberberg, T. Pertsch, and F. Lederer, Journal of the Optical Society of America B **19**, 2637 (2002).

[14] A. B. Aceves, C. De Angelis, T. Peschel, R. Muschall, F. Lederer, S. Trillo, and S. Wabnitz, Physical Review E **53**, 1172 (1996).

[15] D. Cai, A. R. Bishop, and N. Grønbech-Jensen, Physical Review Letters **72**, 591 (1994).

[16] R. Morandotti, U. Peschel, J. S. Aitchison, H. S. Eisenberg, and Y. Silberberg, PHYSICAL REVIEW LETTERS **83**, 4 (1999).

[17] Y. Lahini, A. Avidan, F. Pozzi, M. Sorel, R. Morandotti, D. N. Christodoulides, and Y. Silberberg, Physical Review Letters **100**, 013906 (2008).

[18] L. Martin, G. D. Giuseppe, A. Perez-Leija, R. Keil, F. Dreisow, M. Heinrich, S. Nolte, A. Szameit, A. F. Abouraddy, D. N. Christodoulides, et al., p. 11 (2011).

[19] R. Morandotti, U. Peschel, J. S. Aitchison, H. S. Eisenberg, and Y. Silberberg, Physical Review Letters **83**, 4756 (1999).

[20] T. Pertsch, P. Dannberg, W. Elflein, A. Bräuer, and F. Lederer, Physical Review Letters **83**, 4752 (1999).

[21] B. M. Breid, D. Witthaut, and H. J. Korsch, New Journal of Physics **8**, 110 (2006).

[22] F. Dreisow, A. Szameit, M. Heinrich, T. Pertsch, S. Nolte, A. Tünnermann, and S. Longhi, *Physical Review Letters* **102** (2009).

[23] S. Longhi, M. Marangoni, M. Lobino, R. Ramponi, P. Laporta, E. Cianci, and V. Foglietti, *Physical Review Letters* **96**, 243901 (2006).

[24] K. Hizanidis, Y. Kominis, and N. K. Efremidis, *Optics Express* **16**, 18296 (2008).

[25] S. Minardi, F. Eilenberger, Y. V. Kartashov, A. meit, U. Röpke, J. Kobelke, K. Schuster, H. Bartelt, S. Nolte, L. Torner, et al., *Physical Review Letters* **105** (2010).

[26] D. Mihalache, D. Mazilu, F. Lederer, and Y. S. Kivshar, *Physical Review E* **78** (2008).

[27] D. Mihalache, D. Mazilu, F. Lederer, and Y. S. Kivshar, *Physical Review A* **77** (2008).

[28] S. Longhi, *Optics Letters* **35**, 235 (2010).

[29] S. Longhi, *Physical Review B* **81** (2010).

[30] R. Keil, A. Perez-Leija, F. Dreisow, M. Heinrich, H. Moya-Cessa, S. Nolte, D. N. Christodoulides, and A. Szameit, *Physical Review Letters* **107**, 103601 (2011).

[31] A. Marini, S. Longhi, and F. Biancalana, *Physical Review Letters* **113**, 150401 (2014).

[32] T. X. Tran, S. Longhi, and F. Biancalana, *Annals of Physics* **340**, 179 (2014).

[33] M. O. Williams and J. N. Kutz, *Optical and Quantum Electronics* **44**, 247 (2012).

[34] X. Zhang, X. Yuan, W. Xu, and W. Ye, *Optics Express* **25**, 31204 (2017).

[35] A. Block, C. Etrich, T. Limboeck, F. Bleckmann, E. Sörgel, C. Rockstuhl, and S. Linden, *Nature Communications* **5**, 3843 (2014).

[36] L. Pezzi, L. De Sio, A. Veltri, A. Cunningham, A. De Luca, T. Bürgi, C. Umeton, and R. Caputo, *Nanoscale* **11**, 17931 (2019).

[37] T. X. Tran and F. Biancalana, *Physical Review Letters* **110** (2013).

[38] V. I. Karpman, *Phys. Rev. E* **47**, 2073 (1993).

[39] S. Roy, S. K. Bhadra, and G. P. Agrawal, *Opt. Lett.* **34**, 2072 (2009).

[40] W. Królikowski and S. A. Holmstrom, *Optics Letters* **22**, 369 (1997).

[41] D. W. Aossey, S. R. Skinner, J. L. Cooney, J. E. Williams, M. T. Gavin, D. R. Andersen, and K. E. Lonngren, *Physical Review A* **45**, 2606 (1992).

[42] B. A. Malomed, *Physical Review E* **58**, 7928 (1998).

[43] C. Anastassiou, M. Segev, K. Steiglitz, J. A. Giordmaine, M. Mitchell, M.-f. Shih, S. Lan, and J. Martin, *Physical Review Letters* **83**, 2332 (1999).

[44] G. Vahala, L. Vahala, and J. Yepez, *Philosophical Transactions of the Royal Society of London. Series A: Mathematical, Physical and Engineering Sciences* **362**, 1677 (2004).

[45] G. C. Katsimiga, P. G. Kevrekidis, B. Prinari, G. Biondini, and P. Schmelcher, *Physical Review A* **97**, 043623 (2018).

[46] S. Stalin, R. Ramakrishnan, and M. Lakshmanan, *Photonics* **8**, 258 (2021).

[47] I. E. Papacharalampous, P. G. Kevrekidis, B. A. Malomed, and D. J. Frantzeskakis, *Physical Review E* **68**, 046604 (2003).

[48] U. Al Khawaja, S. M. Al-Marzoug, H. Bahlouli, and B. Baizakov, *Optics Express* **24**, 18148 (2016).

[49] F. Xiao, P. Zhang, S. Liu, and J. Zhao, *Journal of Optics* **13**, 105101 (2011).

[50] J. Cuevas and J. Eilbeck, *Physics Letters A* **358**, 15 (2006), [nlin/0501050](#).

[51] E. Parasuraman, *Journal of Magnetism and Magnetic Materials* **489**, 165403 (2019).

[52] P. Gao, X. Li, Z.-Y. Yang, W.-L. Yang, and S. Yi, **54**, 135301 (2021).

[53] C. I. Christov, S. Dost, and G. A. Maugin, *Physica Scripta* **50**, 449 (1994).

[54] M. Soljačić, K. Steiglitz, S. M. Sears, M. Segev, M. H. Jakubowski, and R. Squier, *Physical Review Letters* **90**, 254102 (2003).

[55] F. Lederer and Y. Silberberg, *Optics and Photonics News* **13**, 48 (2002).

[56] H. S. Eisenberg, Y. Silberberg, R. Morandotti, and J. S. Aitchison, *Physical Review Letters* **85**, 1863 (2000).

[57] Y. Sakai, R. J. Hawkins, and S. R. Friberg, *Optics Letters* **15**, 239 (1990).

[58] A. Szameit, D. Blömer, J. Burghoff, T. Pertsch, S. Nolte, and A. Tünnermann, *Applied Physics B* **82**, 507 (2006).

[59] I. Pavlov, O. Tokel, S. Pavlova, V. Kadan, G. Makey, A. Turnali, Ö. Yavuz, and F. Ö. Ilday, *Optics Letters* **42**, 3028 (2017).

[60] R. Tewari and K. Thyagarajan, *Journal of Lightwave Technology* **4**, 386 (1986).

[61] A. W. Snyder, *Journal of the Optical Society of America* **62**, 1267 (1972).

[62] See supplemental material at [url will be inserted by publisher] for a URL [url1](#).

[63] See supplemental material at [url will be inserted by publisher] for a URL [url1](#).

[64] K. Blow, N. Doran, and S. Phoenix, *Optics Communications* **88**, 137 (1992).

[65] See supplemental material at [url will be inserted by publisher] for a URL [url1](#).

[66] T. X. Tran and Q. Nguyen-The, *Journal of Lightwave Technology* **34**, 4105 (2016).